Site-selective spectroscopy of Er^{3+} ions in the $Bi_{12}SiO_{20}$ piezoelectric crystal

2001 J. Phys.: Condens. Matter 13 11067

(http://iopscience.iop.org/0953-8984/13/48/330)

INSTITUTE OF PHYSICS PUBLISHING JOURNAL OF PHYSICS: CONDENSED MATTER

J. Phys.: Condens. Matter **13** (2001) 11067–11076 PII: S0953-8984(01)24289-1

Site-selective spectroscopy of Er^{3+} ions in the $Bi_{12}SiO_{20}$ piezoelectric crystal

A Lira C[1], U Caldiño G[1], M O Ramírez[2], J A Sanz-García[2] and L E Bausá[2]

[1] Departamento de Física, Universidad Autónoma Metropolitana-Iztapalapa, PO Box 55-534, 09340 México DF, México
[2] Departamento de Física de Materiales, Universidad Autónoma de Madrid, Cantoblanco, 28049 Madrid, Spain

E-mail: luisa.bausa@uam.es

Received 26 April 2001, in final form 17 September 2001
Published 16 November 2001
Online at stacks.iop.org/JPhysCM/13/11067

Abstract

Site-selective spectroscopy fluorescence experiments (emission and excitation) in the near-infrared region associated with the $^4I_{15/2} \leftrightarrow {}^4I_{11/2}$ transitions of Er^{3+} ions have been successfully used to show the presence of two different Er^{3+} centres in the $Bi_{12}SiO_{20}$ piezoelectric crystal. Green (545–570 nm), red (650–690 nm) and near-infrared (850–890 nm) up-converted emissions have been observed and resolved for each type of centre under excitation up to the $^4I_{11/2}$ state. The Stark energy level schemes of the three lower energy states of Er^{3+} ions have been determined and compared for both centres, showing two quite different crystalline field environments. The mechanisms responsible for the up-conversion process (excited state absorption and/or energy transfer up-conversion) are also analysed.

1. Introduction

The interest in the $Bi_{12}SiO_{20}$ (BSO) piezoelectric crystal doped with RE^{3+} ions has increased because of its favourable photoconductive, photorefractive, electro-optic and magneto-optic properties for laser light control [1–3]. Particular attention has been paid to the influence of different dopant elements to optimize the optical properties on the basis of practical applications [4, 5]. Recently, this crystal has been shown to be a very attractive matrix since stimulated Raman scattering and laser action at room temperature were demonstrated when it was activated with Nd^{3+} ions [6].

The $Bi_{12}SiO_{20}$ crystal has the body centred cubic structure known as sillenite. The elementary cubic cell consists of two structural units, SiO_4 tetrahedral (located at the corners and centre of the cube) and BiO_n distorted octahedra ($n = 7$) connecting the SiO_4 groups, being the local symmetry of the Si^{4+} and Bi^{3+} cations T and C_1, respectively. Crystals grown in

non-stoichiometric composition slightly deviated from the molar 6:1 proportion and about 9% of bismuth excess is present in the lattice. Intrinsic defects are then generated by this excess of Bi^{3+} in the lattice. Some authors accept that some of the Si vacancies in the tetrahedral position are occupied by Bi^{3+} atoms, which causes the appearance of ion-vacancy complexes as compensation charge mechanisms [7]. The intrinsic defects, as well as impurity doping, play an important role in the optical behaviour of the material. It has been established that Ln^{3+} ions, in particular Nd^{3+} ions, occupy six-fold oxygen coordination Bi^{3+} distorted crystallographic sites with C_1 symmetry [6]. Some authors, however, have reported the presence of a quite different additional Nd^{3+} centre whose crystal field symmetry is nearly cubic [8].

In this paper the optical properties of a singly Er^{3+} doped $Bi_{12}SiO_{20}$ crystal are studied for the first time to our knowledge. The spectroscopy of Er^{3+} ions in a large variety of systems has been the subject of an overwhelming number of studies since these ions exhibit exceptional suitability for optical amplifiers in long-distance and high bit-rate optical communications. Moreover, Er^{3+} ions are known for their efficient up-conversion of infrared to visible radiation, which could be useful for a number of potential applications [9, 10] or, in contrast, lead to important losses when considering laser gain in the infrared region [11, 12]. Because of their rich energy level scheme multi-photon processes leading to up-conversion have been observed under different excitation wavelengths in a large variety of Er^{3+} doped hosts and laser action from up-converted radiation has been demonstrated [13, 14].

The most common up-conversion mechanisms are: (i) sequential absorption of pump photons in one ion involving excited state absorption (ESA) and (ii) energy transfer up-conversion between two excited Er^{3+} ions (ETU) [15, 16].

In this paper we present a study of the fluorescence of Er^{3+} ions in BSO crystals under excitation in the near-infrared region (950–1000 nm) at low temperature. Infrared emission, as well as up-converted emissions, have been studied. Since the different Er^{3+} centres can play an important role in the optical properties of Er:BSO the identification of the non-equivalent Er^{3+} crystal field centres is an essential task. Thus, site-selective spectroscopy measurements have been used to determine the presence of such non-equivalent Er^{3+} centres in our system, as a needed step for a complete understanding of the optical behaviour of the material. The mechanisms responsible for the up-conversion processes (ESA and/or ETU) are also analysed for the two different types of detected Er^{3+} centres.

2. Experimental details

A single Er^{3+}:$Bi_{12}SiO_{20}$ crystal was grown from stoichiometric melt by the Czochralski technique using platinum crucibles. Bi_2O_3 and SiO_2 were used as starting products. The dopant was placed in the melt in the form of Er_2O_3 oxide.

For the experiments an optically homogeneous $4 \times 4 \times 1$ mm^3 prism was cut and polished to optical quality. The erbium to bismuth concentration in the sample was around 0.3 at% according to x-ray fluorescence analysis.

The emission spectra were studied at low temperature (11 K) by using a closed-cycle He cryostat. An Ar^+ pumped tunable cw Ti–sapphire laser, providing 300 mW at around 990 nm, was focused onto the sample within 0.5 mm and used as the excitation source. The emission from the crystal was dispersed by a 0.5 m focal length monochromator and detected with a cooled photomultiplier. Finally, a lock-in amplifier PAR EG&G (model 5209) was used to improve the signal to noise ratio.

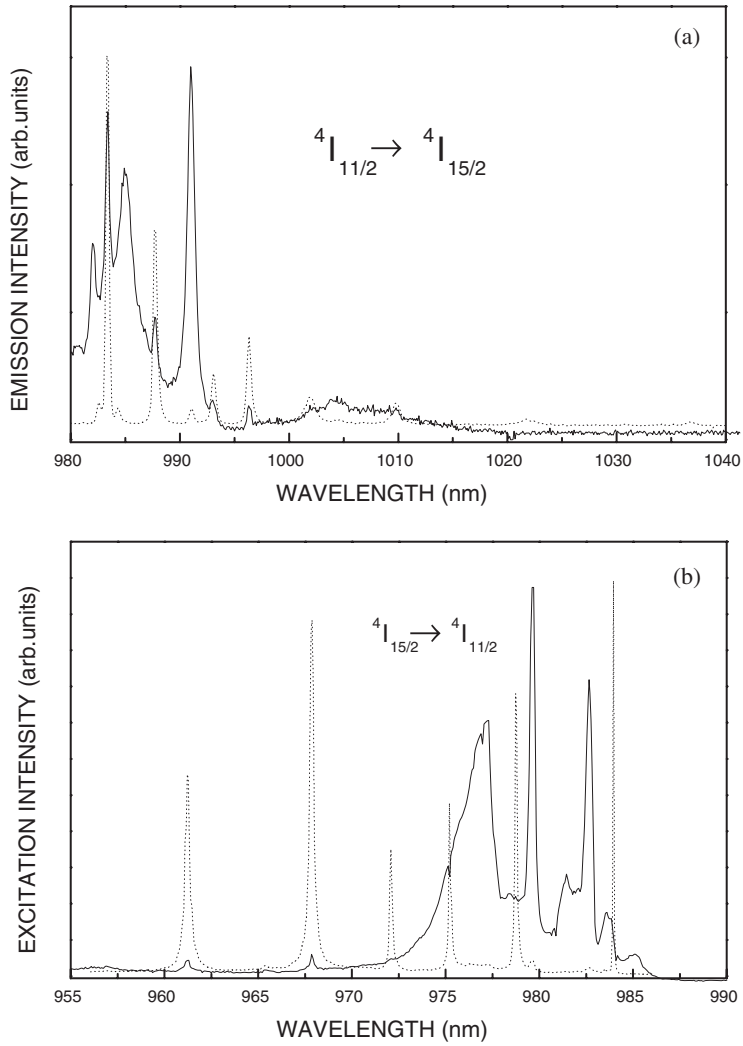

Figure 1. Low temperature site-selective fluorescence spectra of Er^{3+} ions in BSO related to the $^4I_{11/2} \leftrightarrow {}^4I_{15/2}$ transition. (a) Emission spectra: (- - - -) Er_I centre, $\lambda_{exc} = 967.5$ nm and (——) Er_{II} centre, $\lambda_{exc} = 977$ nm; (b) Excitation spectra: (- - - -) Er_I centre, $\lambda_{em} = 996$ nm and (——) Er_{II} centre, $\lambda_{em} = 991$ nm.

3. Results and discussions

3.1. IR luminescence

High-resolution site-selective laser spectroscopy at 11 K was used to study the $^4I_{11/2} \leftrightarrow {}^4I_{15/2}$ transitions of Er^{3+} ions and to investigate the presence of non-equivalent Er^{3+} centres. Thermal population of the excited Stark sublevels of the $^4I_{11/2}$ ($^4I_{15/2}$) state is not expected at 11 K, which notably simplifies the emission (excitation) spectra and allows us to obtain better information on the optical transitions associated with each Er^{3+} centre.

Figure 1(a) shows the low temperature emission spectra associated with the $^4I_{11/2} \rightarrow {}^4I_{15/2}$ transition of Er^{3+} ions in the near-infrared region (980–1040 nm) under excitation at two

different wavelengths up to the $^4I_{11/2}$ state, at 967.5 and 977 nm. The spectra are very different, suggesting the presence of two non-equivalent Er^{3+} centres, hereafter labelled as Er_I and Er_{II} for the emissions obtained after excitation at 967.5 and 977 nm, respectively. For the sake of clarity the spectra of figure 1 show normalized intensities though the actual intensity coming from Er_{II} centres is around a factor of 10 lower than that from Er_I centres. From the emission spectrum related to the Er_I centre eight emission lines are clearly observed, in agreement with a full crystal-field splitting of the $^4I_{15/2}$ ground state into eight Kramers doublets. The crystal-field splitting scheme of the $^4I_{15/2}$ fundamental state for this centre can be obtained from its emission spectrum in figure 1(a), and it has been depicted in figure 2. However, on the spectrum associated with the Er_{II} centre not all the inter-Stark transitions were detected, due to their lower emission intensity and the inferior performance of the detection system at the lower energy region. Then, from here just a partial Stark energy level scheme of the fundamental state for the Er_{II} centres can be obtained.

The low temperature excitation spectra of the emissions displayed in figure 1(a) for each Er^{3+} centre are shown in figure 1(b). The spectra were taken within the $^4I_{11/2} \rightarrow {}^4I_{15/2}$ transitions of the Er_I and Er_{II} centres, monitoring the emissions at 996 and 991 nm, respectively. As observed, the shape of the spectra and the amount of the energy level splitting are substantially different for both centres. Six bands clearly resolved are observed from the excitation spectrum associated with the Er_I centre, in accordance with the number of Stark components of the $^4I_{11/2}$ state in a non-cubic crystal-field symmetry site. The same number of lines can be detected for the Er_{II} centres though, in this case, the spectrum show a poorer resolution. The crystal-field splitting schemes of the $^4I_{11/2}$ state can be obtained from the spectra of figure 1(b) and they have been depicted in figure 2 for each type of centre. The results show that the energy level splitting associated with Er_I centres is clearly stronger when compared to that associated with Er_{II} centres. Thus, two quite different crystal-field symmetry sites should be invoked to account for the presence of these non-equivalent Er^{3+} centres in the matrix.

The existence of these two Er centres could be related to the two different Bi^{3+} available sites in the lattice. Since, according to previous results [6], rare earth ions seem to occupy mainly the distorted Bi^{3+} octahedral site with C_1 local symmetry, in our system the Er_I centre could be tentatively assigned to this symmetry site. The presence of Bi^{3+} atoms in tetrahedral Si vacancies and ion-vacancy complexes could justify the existence of the additional location for Er ions in the BSO crystal. Though site-selective spectroscopy has clearly shown the presence of non-equivalent Er centres in this system, their definitive nature cannot be determined from optical measurements alone, and additional experiments involving electron paramagnetic resonance or RBS/channelling measurements are needed.

3.2. Up-converted luminescence

Up-converted emission in the green (545–570 nm), red (650–690 nm) and near-infrared (850–890 nm) regions is observed under excitation up to the $^4I_{11/2}$ state. As expected, the presence of two different Er centres is detected again on the up-converted emission spectra. Figures 3(a)–(c) show the site-selective up-converted emission spectra at low temperature for two different excitation wavelengths, 967.5 and 977 nm, related to the Er_I and Er_{II} centres, respectively. As in other Er^{3+} compounds [17, 18], the green and red up-converted emissions can be associated with transitions from the $^4S_{3/2}$ and $^4F_{9/2}$ states to the $^4I_{15/2}$ ground state, respectively. The near-infrared up-converted emission can be attributed to the $^4S_{3/2} \rightarrow {}^4I_{13/2}$ transition.

From the spectra associated with the Er_I centre eight well resolved lines are clearly detected in the green and red up-converted emission spectra, in good agreement with the splitting of the $^4I_{15/2}$ ground state, already determined from the direct emission from the $^4I_{11/2}$ state of this cen-

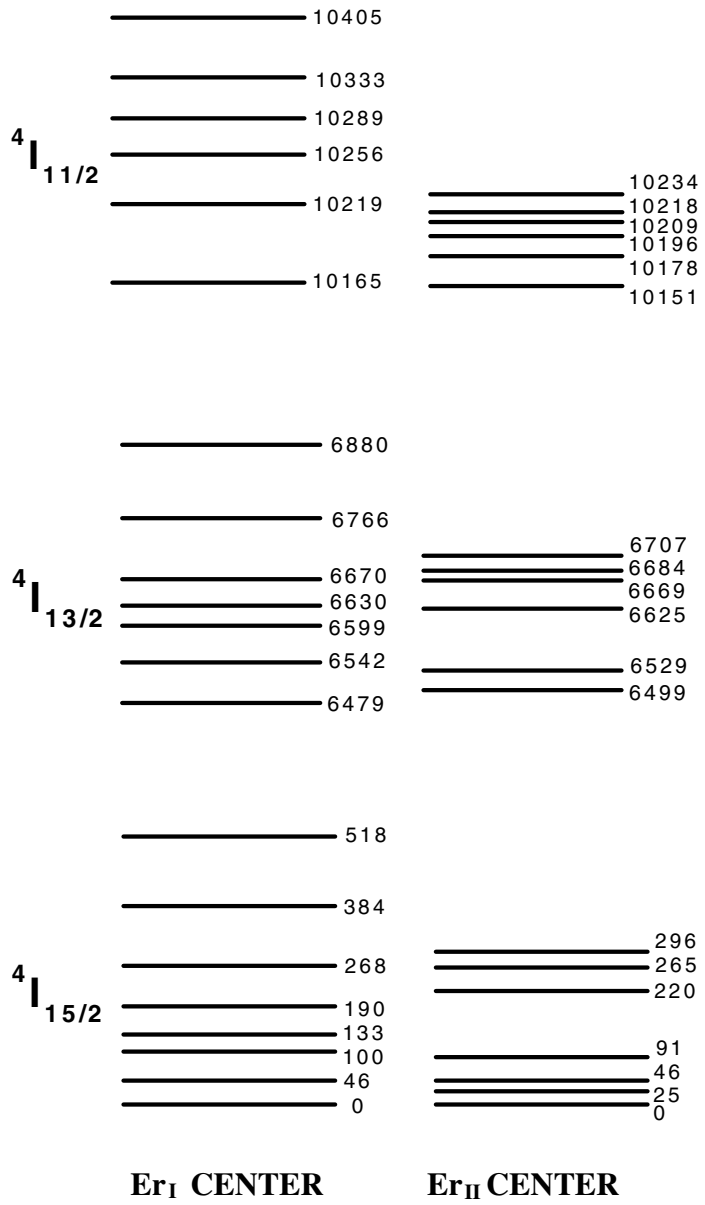

Figure 2. Crystal-field splitting schemes associated with Er_I and Er_{II} centres.

tre. In the near-infrared region seven lines are observed, corresponding to a full splitting of the $^4I_{13/2}$ state. The emission spectra associated with the Er_{II} centre show, in all cases, a poorer resolution and not all the Stark transitions can be identified. The ground state splitting of the $^4I_{15/2}$ for this centre could be determined from the green and red up-conversion emissions, completing the partial information obtained from the direct $^4I_{11/2} \rightarrow {}^4I_{15/2}$ emission. From the emission spectra of figure 3 the Stark energy levels of the $^4I_{13/2}$ state can also be obtained. The crystal field energy level diagram for both centres is shown in figure 2. As observed, the Stark splittings of the states associated with Er_I centres are substantially greater than those of Er_{II} centres,

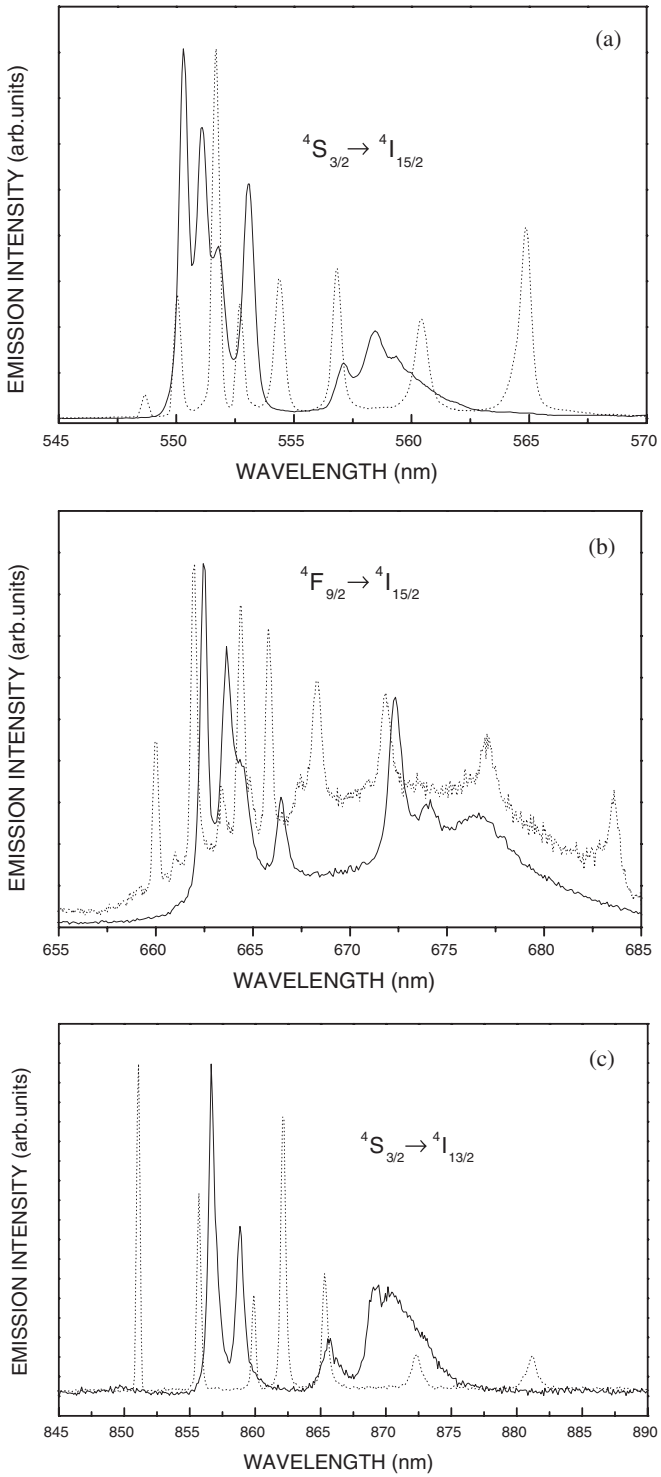

Figure 3. Low temperature site-selective up-converted emission spectra related to the (a) $^4S_{3/2} \rightarrow {}^4I_{15/2}$, (b) $^4F_{9/2} \rightarrow {}^4I_{15/2}$ and (c) $^4S_{3/2} \rightarrow {}^4I_{13/2}$ transitions. (- - - -) Er_I centre and (——) Er_{II} centre. The emission intensities for both centres have been normalized.

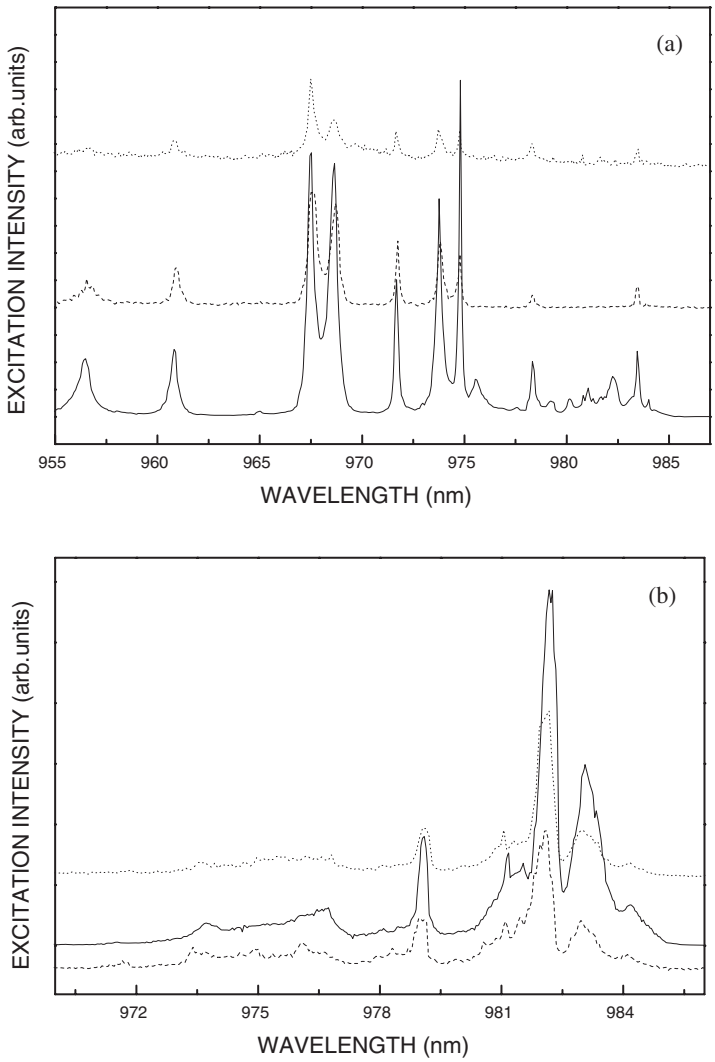

Figure 4. Low temperature excitation spectra monitoring the up-converted emissions from: (a) Er_I centre, (——) $\lambda_{em} = 564.9$ nm, (- - - -) $\lambda_{em} = 660$ nm and (· · · · · ·) $\lambda_{em} = 851$ nm; (b) Er_{II} centre, (——) $\lambda_{em} = 551$ nm, (- - - -) $\lambda_{em} = 662$ m and (· · · · · ·) $\lambda_{em} = 856.7$ nm.

indicating that the location for Er_I centres correspond to a more distorted environment than that of Er_{II} centres. This could justify the assignment of the Er_I centre to the available C_1 local symmetry site. Additionally, a higher oscillator strength could be expected for the more distorted location of the Er_I centre, justifying the higher intensity detected in the fluorescence spectra.

The intensity dependence of the three up-converted emissions on the excitation power was determined to be nearly quadratic for both centres, according to the two-photon character of up-converted emissions. After excitation up to the $^4I_{11/2}$ state a second excitation photon populates the $^4F_{7/2}$ excited state, via ESA, involving one single ion, and/or an ETU process between two Er^{3+} ions excited at the $^4I_{11/2}$ state. Then, the population of the $^4F_{7/2}$ higher state relaxes non-radiatively to the $^4S_{3/2}$ and $^4F_{9/2}$ states, from which the green ($^4S_{3/2} \rightarrow {}^4I_{15/2}$), red ($^4F_{9/2} \rightarrow {}^4I_{15/2}$) and near-infrared ($^4S_{3/2} \rightarrow {}^4I_{13/2}$) up-converted emissions occur.

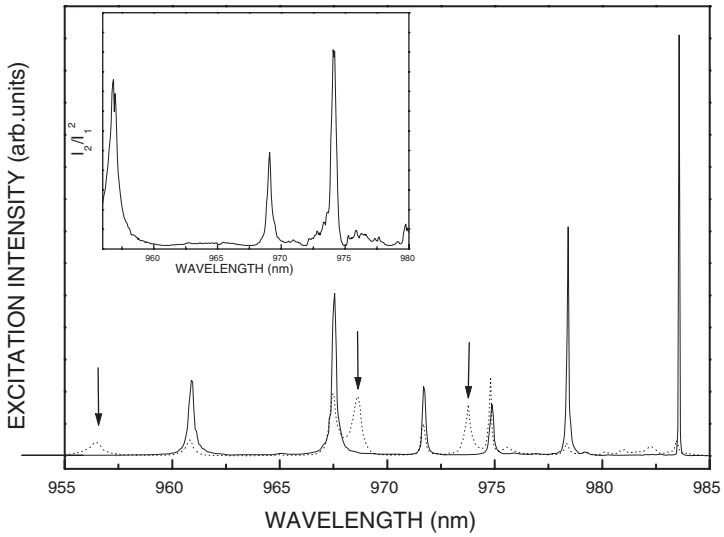

Figure 5. Low temperature excitation spectra of Er_I ions monitoring the one-photon infrared emission ($\lambda_{em} = 991$ nm) and the green up-converted emission ($\lambda_{em} = 564.9$ nm). The inset shows the I_2/I_1^2 ratio versus the input wavelength in the region of the additional bands.

In order to analyse the mechanisms responsible for the up-converted processes (ESA and/or ETU) the excitation spectra have been analysed and compared to those corresponding to the direct $^4I_{11/2} \rightarrow {}^4I_{15/2}$ emission.

Figure 4(a) shows the low temperature excitation spectra of the up-converted emissions associated with the Er_I centre. All these spectra are quite similar, showing the same spectral lines. This suggests that basically the same mechanisms are involved in the up-conversion process responsible for the population of the $^4F_{7/2}$ excited state, and thus for the three observed up-converted emissions. In all the cases, at least three additional lines are observed when comparing the spectra in figure 4(a) to the excitation spectrum of the direct emission. The comparison is shown in figure 5 where the excitation spectrum of the green up-converted emission, along with that of the direct one-photon $^4I_{15/2} \rightarrow {}^4I_{11/2}$ emission, has been depicted. The additional bands, marked with arrows, can be associated with ESA from the lower energy Stark level of the $^4I_{11/2}$ to three of the four crystal-field levels expected for the $^4F_{7/2}$ state, being the spectrum of convolution of the absorption (excitation) of both states. Then, it can be inferred that ESA is contributing to the excited state population and it is, therefore, a mechanism responsible for the up-conversion process in the Er_I centre.

A more detailed analysis can be performed, taking into account that ETU can also contribute to the population of the emitting states for the Er_I centre. The following rate equation is fulfilled once the steady state is achieved:

$$kN_1^2 + \sigma_p I N_1 - \frac{N_2}{\tau_2} = 0 \tag{1}$$

where N_1 and N_2 are the populations of the 1 ($^4I_{11/2}$) and 2 ($^4S_{3/2}$) excited states, respectively; I is the pump intensity (measured as a flux of incident photons per unit area per unit time); σ_p and k correspond to the ESA cross section and energy transfer rate constant, respectively; and τ_2 is the lifetime value of state 2. If ETU were the dominant process, then $\sigma_p I N_1 \ll kN_1^2$ and

equation (1) is reduced to

$$0 = kN_1^2 - \frac{N_2}{\tau_2}. \tag{2}$$

Now, the ratio of the up-converted luminescence intensity, I_2, and the square of the infrared luminescence intensity, I_1, can be estimated by considering that such intensities are proportional to N_2 and N_1, respectively. Thus, from equation (2)

$$\frac{I_2}{I_1^2} \propto \frac{N_2}{N_1^2} = k\tau_2. \tag{3}$$

Therefore, if energy transfer is the dominant process, the quotient I_2/I_1^2 should be constant with the excitation wavelength. As expected, I_2/I_1^2 resulted in being independent of the wavelength, except in the regions in which the additional bands associated with ESA appear. This fact can be visualized from the inset in figure 5, which shows, as an example, the I_2/I_1^2 ratio versus the input wavelength for the Er_I ion green up-converted emission in the region of the additional bands. A similar model and similar results are obtained for the three up-converted emissions. Therefore, the up-converted emissions observed can be attributed to a combination of ESA and ETU processes.

The excitation spectra of the up-converted emissions associated with the Er_{II} centre are shown in figure 4(b). In this case, these spectra can be compared well to the excitation spectrum of the direct infrared emission of the Er_{II} centre and no additional lines are clearly observed. Thus, though ETU could be the dominant mechanism for the up-conversion process in these type of centres, the ESA process cannot be disregarded, since for this centre the low crystal-field splitting and the low emission intensity give rise to a poor resolution in the spectra, which could mask the possible ESA transitions to the $^4F_{7/2}$ excited state.

It should be pointed out that energy transfer between both centres is not an important mechanism since the excitation spectrum of one centre basically does not show absorption lines from the other one.

A dynamical study of the fluorescence is now being made to determine the contribution of each mechanism to the up-conversion processes for each type of centre.

4. Conclusions

The presence of two different Er^{3+} crystal-field centres (Er_I and Er_{II} centres) has been clearly shown in a BSO crystal by site-selective optical spectroscopy. Green ($^4S_{3/2} \rightarrow {}^4I_{15/2}$), red ($^4F_{9/2} \rightarrow {}^4I_{15/2}$) and near-infrared ($^4S_{3/2} \rightarrow {}^4I_{13/2}$) up-converted emissions have been observed after excitation up to the $^4I_{11/2}$ state and resolved for each type of Er centre in the crystal. For the Er_I centre it is possible to conclude that up-converted emissions can be attributed to both ESA and ETU processes. The Stark energy level scheme has been obtained for the $^4I_{15/2}$, $^4I_{13/2}$ and $^4I_{11/2}$ states for both types of centres, showing quite different crystal-field symmetry sites. According to previous results on other rare-earth trivalent ions in this crystal, one of these Er centres could be associated with a C_1 symmetry distorted octahedral Bi^{3+} site. The non-stoichiometry of the crystal and the presence of Si vacancies could favour the presence of the additional Er centre.

Acknowledgments

This work has been supported by the Comisión Interministerial de Ciencia y Tecnología (Spain) under project no PB 97-0033. UC gratefully acknowledges the CONACyT (México) for his sabbatical year grant no 990511.

References

[1] Gunter P 1982 *Phys. Rep.* **93** 199
[2] Rajbenbach H and Huignard J 1985 *Opt. Lett.* **10** 137
[3] Solymar L, Webb D J and Grunnet-Jepsen A 1996 *The Physics and Applications of Photorrefractive Materials* (Oxford: Clarendon)
[4] Arizmendi L, Cabrera J and Agulló-López F 1992 *Int. J. Optoelectron.* **7** 149
[5] Marinova V, Veleva M, Petrova D, Kourmoulis I M, Papazoglou D G, Apostolidis A G, Vanidhis E D and Deliolanis N C 2001 *J. Appl. Phys.* **89** 2686
[6] Kaminskii A A, Bagaev S N, García Solé J, Eichler H J, Fernández J, Jaque D, Findeisen J, Balda R and Agulló Rueda F 1999 *Quantum Electron.* **29** 6
[7] Oberschmid R 1985 *Phys. Status Solidi* a **89** 263
[8] Bondarev A D, Leonov E I, Nyavro A V and Chaldyshev V A 1984 *Opt. Spectrosc. (USSR)* **56** 518
[9] Length W and Macfarlane R M 1992 *Opt. Photon. News* **3** 8
[10] Downining E, Hesselink L, Ralston J and Macfarlane R 1987 *Science* **273** 1185
[11] Koetke J and Huber G 1995 *Appl. Phys.* B **61** 151
[12] Doualan J L, Le Boulanger P, Girard S, Margerie J, Ermneneux F S and Moncorgé R 1997 *J. Lumin.* **72–4** 179
[13] Hebert T, Wannemacher R, Length W and Macfarlane R M 1990 *Appl. Phys. Lett.* **57** 172
[14] Mcfarlane R A 1989 *Appl. Phys. Lett.* **54** 2301
[15] Auzel F E 1973 *Proc. IEEE* **61** 758
[16] Wright J C 1976 *Top. Appl. Phys.* **15** 239
[17] Hehlen M P, Frei G and Güdel H U 1994 *Phys. Rev.* B **50** 16 264
[18] Wenger O S, Gamelin D R and Güdel H U 1999 *Phys. Rev.* B **60** 5312